Journal of Nuclear Materials 448 (2014) 412–419

Contents lists available at ScienceDirect

Journal of Nuclear Materials

journal homepage: www.elsevier.com/locate/jnucmat

Fission product release and survivability of UN-kernel LWR TRISO fuel ☆

T.M. Besmann [a,*], M.K. Ferber [a], H.-T. Lin [a], B.P. Collin [b]

[a] Oak Ridge National Laboratory, P.O. Box 2008, Oak Ridge, TN 37831-6063, United States
[b] Idaho National Laboratory, P.O. Box 1625, Idaho Falls, ID 83415-3955, United States

ARTICLE INFO

Article history:
Available online 31 October 2013

ABSTRACT

A thermomechanical assessment of the LWR application of TRISO fuel with UN kernels was performed. Fission product release under operational and transient temperature conditions was determined by extrapolation from fission product recoil calculations and limited data from irradiated UN pellets. Both fission recoil and diffusive release were considered and internal particle pressures computed for both 650 and 800 μm diameter kernels as a function of buffer layer thickness. These pressures were used in conjunction with a finite element program to compute the radial and tangential stresses generated within a TRISO particle undergoing burnup. Creep and swelling of the inner and outer pyrolytic carbon layers were included in the analyses. A measure of reliability of the TRISO particle was obtained by computing the probability of survival of the SiC barrier layer and the maximum tensile stress generated in the pyrolytic carbon layers from internal pressure and thermomechanics of the layers. These reliability estimates were obtained as functions of the kernel diameter, buffer layer thickness, and pyrolytic carbon layer thickness. The value of the probability of survival at the end of irradiation was inversely proportional to the maximum pressure.

1. Introduction

Historically, nitride-based nuclear fuel has been considered for liquid metal fast breeder reactors, space nuclear propulsion, and gas-cooled reactors. It has not generally been of interest for conventional light water reactors (LWRs) due to its susceptibility to reactions with water and air. Recently, the goal of developing an accident-tolerant fuel (ATF) that meets the objectives of fuel-related core materials tolerant to LWR beyond-design-basis accidents has included evaluating new fuel compositions other than urania. A new concept for LWR nuclear fuel utilizes tri-structural isotropic (TRISO) fuel particles embedded in a SiC matrix in pellet form, replacing sintered urania pellets [1,2]. The fuel is considered significantly more accident tolerant than urania, as the SiC matrix and TRISO particles would be highly resistant to oxidation and fission product release under beyond-design-basis accident conditions. TRISO fuel UN kernels with densities of ~95% are being considered to obtain higher fissile loading compared to UO_2, which is likely needed for the concept.

Another approach being explored is a protected UN fuel pellet within either metallic or SiC cladding. In this case UN fuel offers a significant economic advantage due to its high uranium concentration compared to UO_2. However, the significant adverse reaction of UN with water at reactor temperatures (~300 °C) [3] requires increasing the resistance of UN to high temperature water and steam, and thus using UN grain-level coatings of U_3Si_2 is being separately explored.

The focus of the current paper is on the use of UN kernels in TRISO fuel particles for ATF. To obtain the greatest fissile loading there is an interest in minimizing the amount of structural material while maximizing fissile content. That has translated to increasing enrichment to 19.4%, expanding the kernel diameter beyond the conventional 500 μm, and to efforts to minimize the thicknesses of the low density carbon (buffer) and high density inner pyrolytic carbon (IPyC) layers in the particle. Even with kernel swelling and a thin debonding gap between the buffer and IPyC layer, the initial buffer layer thickness governs the ultimate particle internal pressure as it provides open volume for released fission product gas and vapor. The initial buffer void volume – directly related to the initial buffer thickness – is re-distributed to the expanding kernel void, the shrinking buffer void, and the developing buffer-IPyC gap throughout irradiation, but the total void volume is essentially constant, considering the IPyC inner radius does not practically change. The internal pressure increases under burnup at high temperatures as the gas and vapor evolve and escape to the buffer region, and can eventually fail the particle if it exceeds the strength of the coatings. Thus the minimum buffer layer thickness required

☆ Notice: This manuscript has been authored by UT-Battelle, LLC, under Contract No. DE-AC05-00OR22725 with the U.S. Department of Energy. The United States Government retains and the publisher, by accepting the article for publication, acknowledges that the United States Government retains a non-exclusive, paid-up, irrevocable, world-wide license to publish or reproduce the published form of this manuscript, or allow others to do so, for United States Government purposes.

* Corresponding author. Tel.: +1 865 574 6852.
E-mail address: besmanntm@ornl.gov (T.M. Besmann).

0022-3115/$ - see front matter © 2013 Elsevier B.V. All rights reserved.
http://dx.doi.org/10.1016/j.jnucmat.2013.10.034

depends on the dimensions and history of the particle, including the expected fission product release from the kernel into the buffer volume.

The TRISO particles will be embedded in a SiC matrix, which is currently prepared by nano-powder infiltration and transient eutectic phase (NITE) processing [4,5]. The NITE SiC matrix has dense, isotropic grains which measure several hundred nanometers in diameter. The material has demonstrated excellent irradiation stability [6,7]. Compacts will be formed by hot-pressing the TRISO particles with the NITE matrix to form LWR-sized fuel pellets. These can then be used with conventional or advanced cladding as direct replacement for urania fuel in LWRs. Proposed fuel will utilize an enrichment of 19.4% (this example), with current irradiation conditions envisioned as resulting in a fast fluence of 18×10^{25} n/m^2. Significant efforts are ongoing on both further design of the fuel system and assessment of its use in LWRs.

The current study undertakes to estimate fission product release from a UN kernel and resultant internal particle pressure. The pressure values are used in thermomechanical modeling to determine survival probabilities of particles for several sets of geometries (coating thicknesses). Issues such as swelling[1] in pyrocarbon and SiC layers are considered, however the effect of kernel swelling is not addressed, as notably there is no data for high fluence values, and existing data on swelling in UN varies widely. This study therefore models a three-layer mechanical system consisting of the inner and outer pyrocarbon layers sandwiching the SiC layer, and put under stress by fission gas released by the kernel. In a TRISO particle, the shrinkage of the buffer and IPyC layers early in irradiation forms a gap that mechanically isolates the three outer layers from the kernel and buffer. In this analysis, the three-layer system is assumed to remain mechanically isolated. Extensive swelling of the kernel with burn-up, which could lead to the closing of the buffer-IPyC gap and put the kernel/buffer system in mechanical contact with the three-layer system, is not considered here. Also not considered has been the effect of the SiC matrix, which can have a mitigating effect on particle failure.

2. Fission product release

Fission product release data from high density UN fuel is very limited, with the only sources from work with pellet geometries for systems developed for space nuclear power such as that of Weaver et al. [8] and DeCrescente et al. [9], which were summarized and assessed by Storms [10]. Mixed nitrides for potential use in fast breeder reactors have been studied, and fission product release information provided in Bauer et al. [11,12] and Tanaka et al. [13]. The results are also used in FRAPCON-EP to compute swelling and fission gas release from UN fuel [14]. In Bauer et al. [13], the fission product release is dependent on fuel porosity, with that from low porosity fuel (<10 vol.%) expected to be solely from recoil release from the geometric surface, and which they estimates to be ~0.5%.

2.1. Recoil release

Uranium nitride kernels in potential LWR TRISO fuel are expected to be high density, typically in excess of 95% if theoretical density. Thus it is expected that fission recoil will be an important mechanism by which fission products are released from the kernel to the buffer volume at low temperatures where diffusive transport of gaseous fission products is slow. The information of Bauer et al. [13] together with the fuel pellet geometry (5.715 mm dia. × 6.35 mm length) from this study can be used to determine the noble gas (dominated by Xe and Kr) recoil release fraction using a simplified relation in Lewis [15] for a cylindrical pellet

$$f = \frac{1}{4}\frac{S}{V}\alpha \tag{1}$$

where f is the fractional release, S is the pellet surface area, V is the pellet volume, and α is the fission fragment range. To determine the recoil range in UN the approach of Wise [16] was adopted using the precursor isotopes for Kr and Xe of ^{88}Br and ^{135}I, respectively. The fragments were assumed to have mean energies of 101.5 MeV for ^{88}Br and 66.5 MeV for ^{135}I. The ranges were determined from the tables of Northcliffe and Schilling [17], although UN was not included in the tables as one of the media listed. Data was thus taken for material with the same mean atomic number, namely Ag, per Wise [16]. The resulting average range for the Kr and Xe are 5.68 μm and 3.98 μm, respectively. These values agree reasonably with the 10 μm range quoted by Lewis [15] from Olander [18] for the less dense UO_2. The release fractions due to fission recoil for the 650 μm kernel are 0.918% and 1.31% for Xe and Kr respectively, and for the 800 μm kernel are 0.746% and 1.07% for Xe and Kr, respectively. These agree well with the estimated ~0.5% fission product release fraction due to recoil in UN from Bauer et al. [13].

2.2. Diffusive release

At elevated temperatures fission product diffusion is relatively rapid and thus this additional mechanism must be accounted for in predicting gas release to the buffer region. The PARFUME (PARticle Fuel ModEL) code was used to determine the fractional release of fission gases [19]. PARFUME is an advanced gas-cooled reactor fuel performance modeling and analysis code developed at the Idaho National Laborarory (INL). It is an integrated mechanistic code that evaluates the thermal, mechanical, and physico-chemical behavior of fuel particles during irradiation to determine the failure probability of a population of fuel particles given the particle-to-particle statistical variations in physical dimensions and material properties that arise from the fuel fabrication process, accounting for all viable mechanisms that can lead to particle failure.

In PARFUME, the release fraction is calculated according to the Booth equivalent sphere diffusion model [20], which describes the theoretical diffusive release from a sphere. In a fuel kernel, this sphere can be ascribed to the crystallites if the fission gases are considered to be released once they reach the grain boundaries, or it can be a larger structure depending on the path followed by the gas to escape the fuel. There is no definitive answer as to the release mechanism, and any size ranging from a grain to a kernel could practically represent the Booth sphere.

Under reactor conditions, the release fraction of a gaseous species with diffusion coefficient "D" from a sphere of radius "a" after an irradiation time "t" is given by:

$$f = 1 - \frac{6}{90\tau} + \frac{6}{\pi^4\tau}\sum_{n=1}^{\infty}\left(\frac{1}{n^4} * e^{-n^2\pi^2\tau}\right) \tag{2}$$

where $\tau = \frac{Dt}{a^2}$ is the dimensionless diffusion time. PARFUME truncates the infinite series at $n = 100$, which results in a relative precision on the release fraction better than 10^{-8}. It can be shown that for values of τ lower than 0.35, the infinite series can be approximated by:

$$f = \sqrt[4]{\frac{\tau}{\pi}} - \frac{3}{2}\tau \tag{3}$$

which can be further reduced to:

[1] Here swelling refers to fluence-dependent strains developed in in the PyC layers. These strains may be positive (expansion) or negative (contraction or shrinkage).

$$f = \sqrt[4]{\frac{\tau}{\pi}} \tag{4}$$

with a relative error of 10% if $\tau < 0.02$ (a relative error of 1% would be achieved for $\tau < 2 \times 10^{-4}$) [21].

PARFUME considers that the fission gases are released from spheres having a diameter of 20 μm, which is assumed to be of the order of magnitude of the size of UN crystallites. At each irradiation step, PARFUME calculates the kernel temperature T_k and the subsequent fractional release of fission gas, using the effective diffusion coefficient D_g ($cm^{-2}\ s^{-1}$) fitted to Storms [10] correlated fission gas release from UN fuel as reported by Weaver et al. [3] and DeCrescente et al. [9] for fuel with densities ⩾94 vol.% (Fig. 1)

$$D_g = 6.6454 * 10^{-12} * e^{-19164/T} \tag{5}$$

Tanaka et al. [13] utilized low density fuel (84.8% and 86% theoretical density) and thus correlation with the proposed high density (~95%) UN kernels was not viewed as appropriate. For the nominal conditions (enrichment 19.4%, fast fluence $18 * 10^{25}$ n/m^2, irradiation time 1000 EFPD) and geometry (kernel diameter 650 or 800 μm), PARFUME calculates the diffusive release fractions at the end of irradiation. The values were determined for fission gas release at the maximum operating temperature of 800 °C, a design-basis accident temperature of 1250 °C, and a beyond design-basis accident temperature of 1600 °C. At 800 °C the values are 2.2% for the 650 μm kernel and 2.6% for the 800 μm kernel; at 1250 °C for the 650 μm and 800 μm kernels the values are 15.6% and 17.0%, respectively; and at 1600 °C for the 650 μm and 800 μm kernels they are 38.4% and 41.5%, respectively.

2.3. Fission gas inventory and particle pressure

A set of SCALE calculations for a UN kernel enriched to 19.4% ^{235}U in LWR TRISO fuel after George et al., [22] determined the fission product inventory after 19% FIMA over three years. Noble fission gas release values determined from the relations above are shown in Table 1, which are the sum of the fission recoil (in the case of Kr and Xe) and diffusive release. Note that He is assumed to be released solely through a diffusive mechanism. At 800 °C the Xe and Kr release fraction for fission recoil and diffusion are of the same order of magnitude, and at the higher temperatures diffusion dominates. Vapor partial pressures from fuel and fission product phases can be important contributors to the total pressure at these elevated temperatures. Their pressures were determined from equilibrium calculations at temperature assuming the fuel and fission product inventory in a particle and their chemical state, with the free volume assumed to equal 50% of the total buffer layer volume. The calculations were performed using the FactSage thermochemical software [23] and attendant thermochemical databases, with the exception of thermochemical values for UN which were obtained from Besmann et al. [24]. The results are seen in Fig. 2a and b. The noble gases account for about 48–63% of the gas vapor inventory depending on temperature between 800 °C and 1600 °C, with the vapor pressures over the condensed fission products providing the remainder. As the pressures are proportional to available volume, they are seen to remain modest at buffer layer thicknesses >50 μm and temperatures of 800 °C and 1250 °C, whereas they rise sharply at 1600 °C and smaller buffer layer thicknesses.

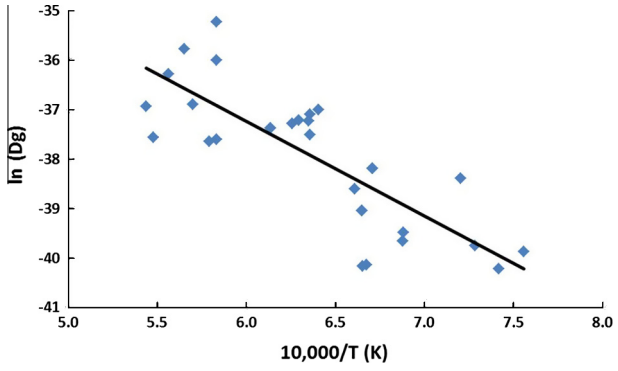

Fig. 1. Noble gas diffusivity from experimental measurements of release from UN pellets as a function of reciprocal temperature from the selected data of Storms [10].

3. Modeling coated particle properties and survivability

In the current study, the stress analyses method developed by Miller [19,25–29] was used to estimate the stress distributions generated within the TRISO particle (Fig. 3 and Table 2) undergoing burnup. In this approach, the stress analyses are applied only to the outer 3 layers, (IPyC, SiC, and OPyC). In other words these three layers are assumed to be structurally isolated from the kernel due to the low elastic modulus of the buffer and the tendency of the elastic moduli of both the buffer and kernel to decrease with increasing irradiation, after Boer et al. [29]. As shown in Fig. 4, the primary external boundary condition that must be applied to this model is the internal pressurization that arises due to gas evolution from the kernel over time. In the present study, this time-dependent pressure, P_i, was calculated using the approach described in Section 2. The stress–strain relationships of Miller [25–28] for the model in Fig. 4 are as follows,

$$\frac{d\varepsilon_r^L}{dt} = \frac{1}{E}\left(\frac{d\sigma_r^L}{dt} - 2\mu\frac{d\sigma_t^L}{dt}\right) + \frac{de_r^L}{dt} + c(\sigma_r^L - 2v\sigma_t) \tag{6}$$

$$\frac{d\varepsilon_t^L}{dt} = \frac{1}{E}\left[\frac{d\sigma_t^L}{dt} - \mu\left(\frac{d\sigma_t^L}{dt} + \frac{d\sigma_r^L}{dt}\right)\right] + \frac{de_t^L}{dt} + c\left[\sigma_t^L - v(\sigma_t^L + \sigma_r^L)\right] \tag{7}$$

where ε is the total strain, σ is the stress, E is the elastic modulus, μ is Poisson's ratio, e is the swelling strain (a function of fluence, t), c is the creep constant with units of strain per fluence per unit stress, and v is a material property that dictates compressibility of the layer under irradiation (approximately equal to 0.5). The subscripts t and r denote the tangential and radial directions, respectively. The superscript L refers to the specific layer (L = IPyC, SiC, or OPyC). For spherical symmetry, the radial and tangential strains listed in Eqs. (8) and (9) are simple functions of the radial displacement, u,

$$\varepsilon_r = \frac{du}{dr} \tag{8}$$

$$\varepsilon_t = \frac{u}{r} \tag{9}$$

In the absence of creep and swelling, the determination of the stress distributions within the layer requires consideration of the stress–strain (Eqs. (6) and (7)), strain–displacement (Eqs. (8) and (9)), and an equilibrium equation. For a purely time-independent elastic material, rearrangement of these three sets of equations leads to a second order differential equation with u as the dependent variable and r as the independent variable. The solution to this differential equation, which applies only to a single layer (material), consists of an expression involving two constants, C1 and C2. If multiple layers are present each with their own values of E and μ, unique sets of constants will be associated with each layer. The specific solution requires determining the value of the constants C1 and C2 for each layer in the system. These solutions are dictated by satisfying the

Table 1
Fractional release from UN kernels of noble gases and total amounts of Xe, Kr, and He based on kernel diameter.

Kernel dia.	650 μm					800 μm				
Temp. (°C)	Xe% release	Kr% release	mol Xe	mol Kr	mol He	Xe% release	Kr% release	mol Xe	mol Kr	mol He
800	3.12%	3.51%	1.069E−08	1.506E−09	8.64E−10	3.35%	3.67%	2.14E−08	2.93E−09	1.90E−09
1250	16.5%	16.9%	5.664E−08	7.086E−09	6.12E−09	17.7%	18.1%	1.13E−07	1.42E−08	1.24E−08
1600	39.3%	39.7%	1.348E−07	1.687E−08	1.51E−08	42.2%	42.6%	2.70E−07	3.38E−08	3.04E−08

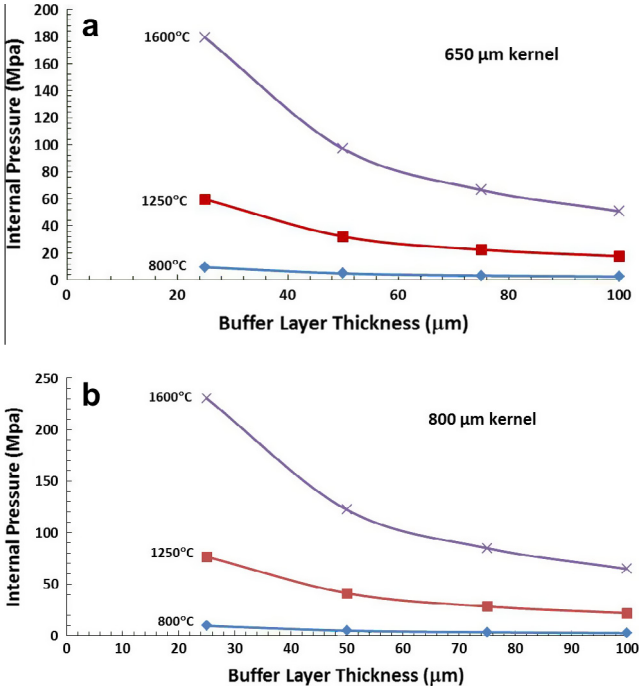

Fig. 2. Computed coated particle internal pressure based on buffer layer thickness and temperature determined from equilibrium gas volume and noble gas release fraction for (a) 650 μm and (b) 800 μm diameter kernels.

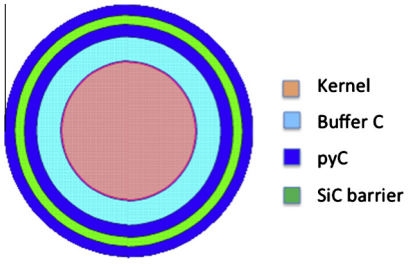

Fig. 3. Schematic representation of TRISO particle. The PyC layers are designated as either inner (IPyC) or outer (OPyC), and the particle diameter is typically ~1 mm.

Table 2
Elastic properties and layer dimensions used for reliability analyses.

	E (MPa)	η	Dimensions (μm)
Kernel	219,000	0.32	650 and 800 (Diameter)
Buffer	11,000	0.23	25, 50, 75, 100 (Thickness)
IPyC	38,070	0.23	10, 15, 20, 25, 30 (Thickness)
SiC	455,000	0.13	35 (Thickness)
OPyC	38,070	0.23	10, 15, 20, 25, 30 (Thickness)

boundary conditions shown in Fig. 4, where P_i and P_o represent inner and outer pressures, respectively.

When creep and swelling/shrinkage processes are active, the solution scheme described by Miller [16–19] can be used to

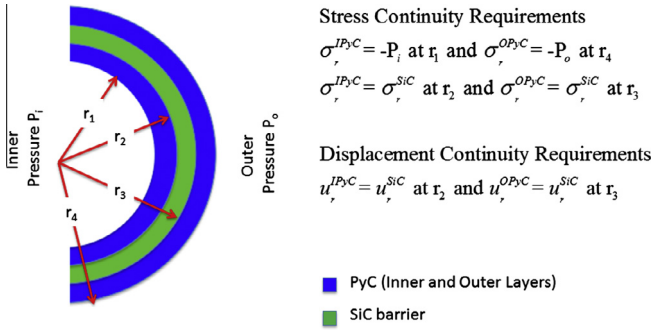

Fig. 4. Boundary conditions for the 3-layer system.

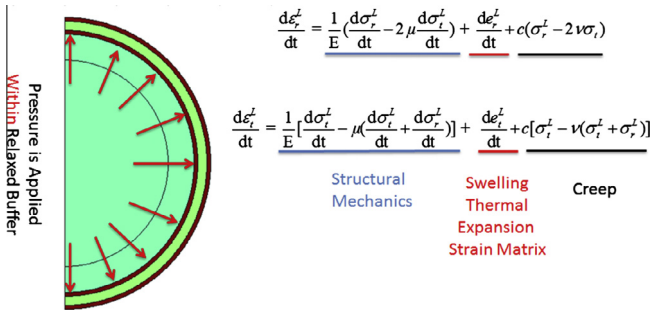

Fig. 5. Stress–strain and strain–displacement relationships are used in accordance with an equilibrium equation to generate a second order differential equation with u as the dependent variable and r as the independent variable.

calculate the stress distributions as a function of fluence. This solution scheme is currently used for the stress calculations in PARFUME [19,25–29]. For this work, a commercial finite element solver, COMSOL Multiphysics software,[2] was used to predict the time dependent stress distributions generated in a TRISO particle as a function of fluence. As its name implies, this software allows one to model a variety of physics-based phenomena such as elastic response (static structural analyses), creep, diffusion, and heat transfer. The key steps in developing a model are (1) define and mesh the geometry (1, 2, and 3 dimensional models are possible), (2) specify the physics, (3) set the appropriate properties for the materials in the model, (4) apply the boundary conditions, (5) solve the model, and (6) visualize the results. Input such as the boundary conditions and material properties can vary with position and/or time or be specified as tabular or analytic functions of the dependent variables. The later aspect allows the user to couple the various physics.

The structural mechanics and creep modules available with the COMSOL software were used to solve for the radial displacements occurring in the model shown in Fig. 5. Swelling/shrinkage was accommodated using time-dependent strain terms in conjunction with the thermal expansion strain matrix available in COMSOL.

[2] Manufactured by COMSOL, Inc., 1 New England Executive Park, Suite 350, Burlington, MA 01803, USA.

Table 3
Summary of benchmarks evaluated in an IAEA report [31]. The designators, (a), (b) and (c) in the conditions column refer to the swelling rate conditions discussed below.

Case	Layers modeled	Conditions
1	SiC	Kernel diameter = 500 μm, buffer thickness = 100 μm, and SiC coating = 35 μm. No creep or swelling. Internal pressure = 25 MPa. Elastic behavior assumed
2	Inner PyC	Same as Case 1 except inner PyC layer (90 μm thickness) replaces SiC layer
3	Inner PyC and SiC	Same as Case 1 except inner PyC layer (90 μm thickness) is added to model
4a	Inner PyC and SiC	Same as Case 3 except constant swelling rate (a) of PyC prescribed
4b	Inner PyC and SiC	Same as Case 3 except constant creep of PyC prescribed
4c	Inner PyC and SiC	Same as Case 3 except constant creep and constant swelling rate (a) of PyC prescribed
4d	Inner PyC and SiC	Same as Case 3 except constant creep and fluence dependent swelling (a) of PyC prescribed.
5	Inner PyC, SiC, and outer PyC	Kernel diameter = 350 μm, buffer thickness = 100 μm, IPyC thickness = 40 μm, SiC coating = 35 μm, and IPyC thickness = 40 μ. Constant creep and fluence dependent swelling (b) of PyC prescribed. Internal pressure ramped linearly from 0 to 15.54 MPa
6	Inner PyC, SiC, and outer PyC	Kernel diameter = 500 μm, buffer thickness = 100 μm, IPyC thickness = 40 μm, SiC coating = 35 μm, and IPyC thickness = 40 μm. Constant creep and fluence dependent swelling (b) of PyC prescribed. Internal pressure ramped linearly from 0 to 26.2 MPa
7	Inner PyC, SiC, and outer PyC	Kernel diameter = 500 μm, buffer thickness = 100 μm, IPyC thickness = 40 μm, SiC coating = 35 μm, and IPyC thickness = 40 μm. Constant creep and fluence dependent swelling (c) of PyC prescribed. Internal pressure ramped linearly from 0 to 26.2 MPa
8	Inner PyC, SiC, and outer PyC	Kernel diameter = 500 μm, buffer thickness = 100 μm, IPyC thickness = 40 μm, SiC coating = 35 μm, and IPyC thickness = 40 μm. Constant creep and fluence dependent swelling (c) of PyC prescribed. Internal pressure was cyclic with fluence

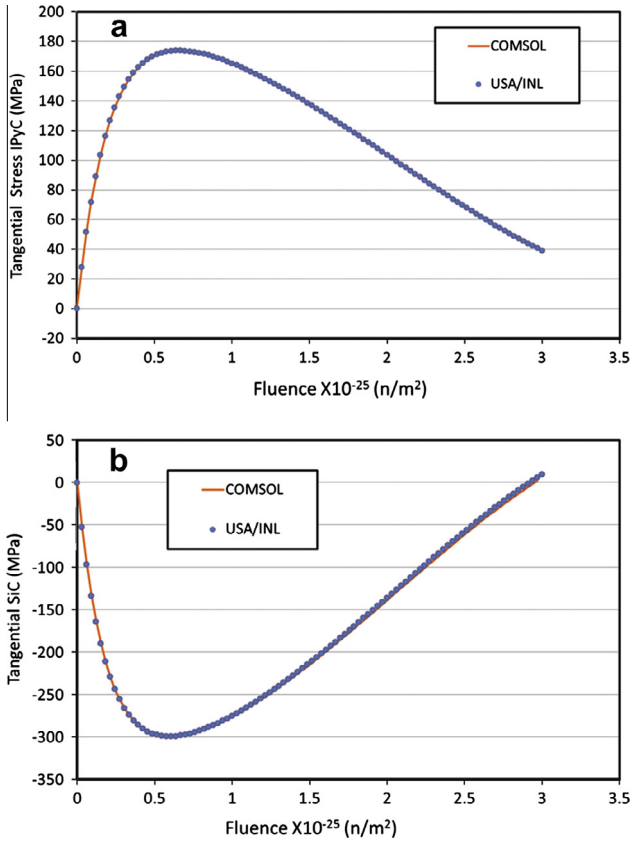

Fig. 6. Comparison of the COMSOL and PARFUME stress-fluence profiles calculated for Case 7. The plot (a) is for the tangential stresses in the PyC layer while the plot (b) is for the tangential stresses in the SiC layer.

To account for pressure build-up within the buffer as determined in Section 2, a time-dependent stress (equal to negative pressure) was prescribed as an "internal stress" boundary condition and applied to the inner surface of the IPyC (Fig. 5). This pressure, which corresponds to the P_i prescribed in Fig. 4, was assumed to increase linearly with fluence to the maximum values determined above, which occurred at a fluence of 3×10^{25} n/m^2, based on 19% FIMA [30]. The outer pressure, P_o, was assumed to be relatively small and constant throughout the transient analyses. Consequently its contribution to the stresses was negligible.

The COMSOL model was validated by comparing the radial and tangential stress-radius profiles predicted by COMSOL with those obtained in a previous International Atomic Energy Agency (IAEA) study [31]. One objective of the study was to validate various predictive methods for the analyses of nuclear fuel behavior. To this

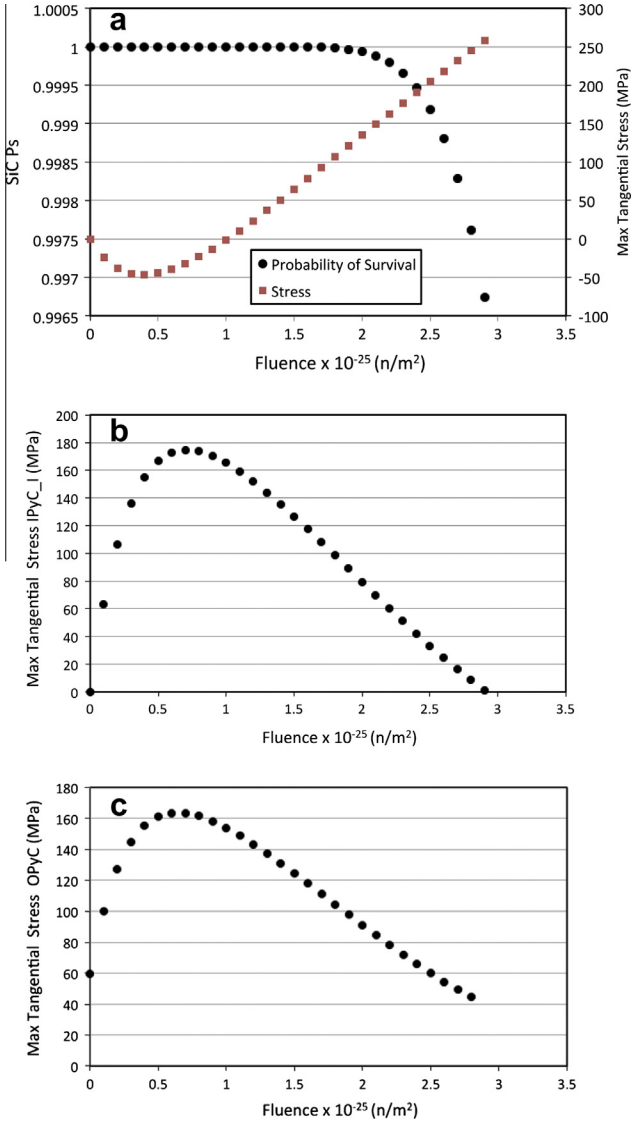

Fig. 7. Examples of fluence dependent stress curves for (a) SiC, (b) 10 μm IPyC, and (c) 10 μm OPyC layers for 650 μm kernel and 25 μm buffer at 1250 °C (1073 K).

end, benchmark calculations were made in order to compare the predictive capabilities of the various codes. The 8 benchmarks used for the single particle analyses are summarized in Table 3. The results determined with COMSOL were compared with the benchmark data generated with the PARFUME code, since the stress analysis in this code is based on the same mathematical equations used in the COMSOL model. Agreement between the COMSOL and PARFUME results were excellent for Cases 1–7 (Case 8 has not been evaluated with COMSOL). For example, Fig. 6 compares results for Case 7 in Table 3.

The values for the creep parameter, which was temperature dependent, and the swelling/shrinkage rates, which are functions of temperature, fluence, and IPyC density, were taken from the work of Miller et al. [19]. The calculation of the swelling/shrinkage rate-fluence curves for the kernel temperatures of 800 °C and 1250 °C required interpolation of the existing data which were available for temperatures of 600 °C, 1032 °C, and 1350 °C. No extrapolation was attempted for the case of the 1600 °C kernel temperature. Instead, the available swelling/shrinkage rate-fluence curves at 1350 °C were assumed to be valid. Finally, at the time of this work the use of fluence-dependent properties within COMSOL had not been developed. As such the elastic properties defined in Table 2 were assumed to remain constant with fluence.

The resulting stress profiles generated within the SiC layer were subsequently used to calculate the probability of survival, P_s, from the expression,

$$P_s = exp\left[-\int\left(\frac{\sigma}{\sigma_o}\right)^m dV\right] \quad (10)$$

where σ is either the radial or tangential stress (both are functions of r), m is the Weibull modulus constant, and σ_o is the Weibull scale parameter. The integration is carried out over the volume, V, for positive values of the radial and tangential stresses. The use of the volume integration assumes that the flaws responsible for failure were located within the bulk. In reality the surface flaws may dominate given the low volume associated with the barrier layer. A more rigorous analyses would require better fractographic data as well as a more complete understanding of the strength-size scaling relationships for the SiC material. The values of m and σ_o were equal to 6 and 500 MPa mm$^{3/6}$, respectively, from Miller et al. [19].

4. Probability of survival of coated particles

Fig. 7 illustrates some typical examples of the fluence dependence of the SiC, IPyC, and OPyC tangential stresses. The initial increase in the PyC tangential stresses with increasing fluence is due to the combined effects of pressure increase within the kernel region and swelling (or shrinkage) of the IPyC layer. However as the stress increases, the contribution of creep induced stress relaxation also increases such that the tangential stress versus fluence curve exhibits a maximum, in this case at a fluence of 0.65. A second effect of creep relaxation in the IPyC layer is that the SiC must now support more and more of the internal pressure load. This is reflected in an increase in tangential stress in the SiC and ultimately a decrease in the probability of survival. The value of P_s at the end of fluence depends primarily on the maximum pressure.

Tables 4 and 5 summarize the probabilities of survival and maximum PyC tangential stresses for the 650 and 800 μm kernels as a function of buffer thickness, PyC thickness, and maximum pressure. One can evaluate the acceptable conditions for particle survivability by specifying a minimum P_s for SiC and a maximum allowable stress for the PyC (σ_{PyC}). Table 6 summarizes the

Table 4
Summary of SiC probabilities of survival for the 650 and 80 μm kernels as a function of buffer thickness, PyC thickness, and maximum pressure.

Probabilities of survival Kernel diameter = 650 μm									
	Pressures			10 μm PyC layers			15 μm PyC layers		
Buffer Thickness (μm)	800 (°C) *P* (MPa)	1250 (°C) *P* (MPa)	1600 (°C) *P* (MPa)	800 (°C) Ps	1250 (°C) Ps	1600 (°C) Ps	800 (°C) Ps	1250 (°C) Ps	1600 (°C) Ps
25	9.46	76.60	230.00	1.0000	0.9991	0.0000	1.0000	0.9993	0.0000
50	4.83	41.20	122.00	1.0000	1.0000	0.9628	1.0000	1.0000	0.9627
75	3.30	28.30	84.90	1.0000	1.0000	0.9933	1.0000	1.0000	0.9935
100	2.55	21.90	64.60	1.0000	1.0000	0.9980	1.0000	1.0000	0.9981
	20 μm PyC layers			25 μm PyC layers			30 μm PyC layers		
Buffer Thickness (μm)	800 (°C) Ps	1250 (°C) Ps	1600 (°C) Ps	800 (°C) Ps	1250 (°C) Ps	1600 (°C) Ps	800 (°C) Ps	1250 (°C) Ps	1600 (°C) Ps
25	1.0000	0.9995	0.0000	1.0000	0.9996	0.0000	1.0000	0.9997	0.2812
50	1.0000	1.0000	0.9628	1.0000	1.0000	0.9631	1.0000	1.0000	0.9634
75	1.0000	1.0000	0.9938	1.0000	1.0000	0.9941	1.0000	1.0000	0.9944
100	1.0000	1.0000	0.9983	1.0000	1.0000	0.9984	1.0000	1.0000	0.9986
Kernel diameter = 800 μm									
	Pressures			10 μm PyC layers			15 μm PyC layers		
Buffer Thickness (μm)	800 (°C) *P* (MPa)	1250 (°C) *P* (MPa)	1600 (°C) *P* (MPa)	800 (°C) Ps	1250 (°C) Ps	1600 (°C) Ps	800 (°C) Ps	1250 (°C) Ps	1600 (°C) Ps
25	7.22	59.60	179.00	1.0000	0.9991	0.0000	1.0000	0.9994	0.0000
50	3.74	32.20	96.90	1.0000	1.0000	0.9604	1.0000	1.0000	0.9612
75	2.59	22.40	66.60	1.0000	1.0000	0.9939	1.0000	1.0000	0.9943
100	2.02	17.60	50.80	1.0000	1.0000	0.9983	1.0000	1.0000	0.9985
	20 μm PyC layers			25 μm PyC layers			30 μm PyC layers		
Buffer Thickness (μm)	800 (°C) Ps	1250 (°C) Ps	1600 (°C) Ps	800 (°C) Ps	1250 (°C) Ps	1600 (°C) Ps	800 (°C) Ps	1250 (°C) Ps	1600 (°C) Ps
25	1.0000	0.9995	0.0000	1.0000	0.9997	0.0000	1.0000	0.9998	0.0000
50	1.0000	1.0000	0.9621	1.0000	1.0000	0.0000	1.0000	1.0000	0.9641
75	1.0000	1.0000	0.9947	1.0000	1.0000	0.9950	1.0000	1.0000	0.9954
100	1.0000	1.0000	0.9986	1.0000	1.0000	0.9988	1.0000	1.0000	0.9989

Table 5
Summary of maximum tangential stresses in the PyC layers for 650 and 800 μm kernels as a function of buffer thickness PyC thickness, and maximum pressure.

Max stresses in PyC layers Kernel diameter = 650 μm									
	Pressures			10 μm PyC layers			15 μm PyC layers		
Buffer Thickness (μm)	800 (°C) *P* (MPa)	1250 (°C) *P* (MPa)	1600 (°C) *P* (MPa)	800 (°C) stmax	1250 (°C) stmax	1600 (°C) stmax	800 (°C) stmax	1250 (°C) stmax	1600 (°C) stmax
25	9.46	76.60	230.00	296	180	129	304	179	126
50	4.83	41.20	122.00	296	183	125	304	188	123
75	3.30	28.30	84.90	296	186	124	303	191	127
100	2.55	21.90	64.60	295	187	126	302	192	129
	20 μm PyC layers			25 μm PyC layers			30 μm PyC layers		
Buffer Thickness (μm)	800 (°C) stmax	1250 (°C) stmax	1600 (°C) stmax	800 (°C) stmax	1250 (°C) stmax	1600 (°C) stmax	800 (°C) stmax	1250 (°C) stmax	1600 (°C) stmax
25	312	185	123	321	191	120	329	197	123
50	311	194	125	319	199	129	329	205	133
75	310	196	130	317	201	134	324	206	137
100	308	197	132	315	202	136	321	206	139
Kernel diameter = 800 μm									
	Pressures			10 μm PyC layers			15 μm PyC layers		
Buffer Thickness (μm)	800 (°C) *P* (MPa)	1250 (°C) *P* (MPa)	1600 (°C) *P* (MPa)	800 (°C) stmax	1250 (°C) stmax	1600 (°C) stmax	800 (°C) stmax	1250 (°C) stmax	1600 (°C) stmax
25	7.22	59.60	179.00	291	184	134	298	180	132
50	3.74	32.20	96.90	293	180	129	299	184	126
75	2.59	22.40	66.60	293	183	127	298	188	124
100	2.02	17.60	50.80	293	185	127	298	189	126
	20 μm PyC layers			25 μm PyC layers			30 μm PyC layers		
Buffer Thickness (μm)	800 (°C) stmax	1250 (°C) stmax	1600 (°C) stmax	800 (°C) stmax	1250 (°C) stmax	1600 (°C) stmax	800 (°C) stmax	1250 (°C) stmax	1600 (°C) stmax
25	304	180	129	311	184	126	317	189	124
50	305	189	123	311	193	124	317	198	126
75	304	192	126	310	196	129	315	200	132
100	303	193	129	308	197	131	314	201	134

Table 6
Summary of acceptable conditions (yes) for the TRISO particle for 650 and 800 μm kernels as a function of buffer thickness, PyC thickness, and maximum pressure.

Acceptable conditions Kernel diameter = 650 μm									
	Pressures			10 μm PyC layers			15 μm PyC layers		
Buffer Thickness (μm)	800 (°C) *P* (MPa)	1250 (°C) *P* (MPa)	1600 (°C) *P* (MPa)	800 (°C) Ps	1250 (°C) Ps	1600 (°C) Ps	800 (°C) Ps	1250 (°C) Ps	1600 (°C) Ps
25	9.46	76.60	230.00	Yes	Yes	No	Yes	Yes	No
50	4.83	41.20	122.00	Yes	Yes	No	Yes	Yes	No
75	3.30	28.30	84.90	Yes	Yes	Yes	Yes	Yes	Yes
100	2.55	21.90	64.60	Yes	Yes	Yes	Yes	Yes	Yes
	20 μm PyC layers			25 μm PyC layers			30 μm PyC layers		
Buffer Thickness (μm)	800 (°C) Ps	1250 (°C) Ps	1600 (°C) Ps	800 (°C) Ps	1250 (°C) Ps	1600 (°C) Ps	800 (°C) Ps	1250 (°C) Ps	1600 (°C) Ps
25	Yes	Yes	No	Yes	Yes	No	Yes	Yes	No
50	Yes	Yes	No	Yes	Yes	No	Yes	Yes	No
75	Yes	Yes	Yes	Yes	Yes	Yes	Yes	Yes	Yes
100	Yes	Yes	Yes	Yes	Yes	Yes	Yes	Yes	Yes
Kernel diameter = 800 μm									
	Pressures			10 μm PyC layers			15 μm PyC layers		
Buffer Thickness (μm)	800 (°C) *P* (MPa)	1250 (°C) *P* (MPa)	1600 (°C) *P* (MPa)	800 (°C) Ps	1250 (°C) Ps	1600 (°C) Ps	800 (°C) Ps	1250 (°C) Ps	1600 (°C) Ps
25	7.22	59.60	179.00	Yes	Yes	No	Yes	Yes	No
50	3.74	32.20	96.90	Yes	Yes	No	Yes	Yes	No
75	2.59	22.40	66.60	Yes	Yes	Yes	Yes	Yes	Yes
100	2.02	17.60	50.80	Yes	Yes	Yes	Yes	Yes	Yes
	20 μm PyC layers			25 μm PyC layers			30 μm PyC layers		
Buffer Thickness (μm)	800 (°C) Ps	1250 (°C) Ps	1600 (°C) Ps	800 (°C) Ps	1250 (°C) Ps	1600 (°C) Ps	800 (°C) Ps	1250 (°C) Ps	1600 (°C) Ps
25	Yes	Yes	No	Yes	Yes	No	Yes	Yes	No
50	Yes	Yes	No	Yes	Yes	No	Yes	Yes	No
75	Yes	Yes	Yes	Yes	Yes	Yes	Yes	Yes	Yes
100	Yes	Yes	Yes	Yes	Yes	Yes	Yes	Yes	Yes

acceptable conditions for the case where $P_s \geqslant 0.99$ and $\sigma_{PyC} \leqslant 350$ MPa. For instance, under the 800 °C operating condition the probability of survival is approximately 100% independent of buffer thickness and PyC thickness for both kernel sizes. Even at 1250 °C the P_s could be $\geqslant 0.99$ under the selected conditions of buffer thickness and PyC thickness for both kernel sizes.

5. Conclusions

The application of TRISO fuel particles in LWRs requires maximizing fuel loading and significant burnup, and hence the need to use UN fuel kernels and minimal TRISO coating layers. Analysis of the survival probability of thus designed particles was undertaken utilizing pressure buildup in the particle as a result of fission gas release. There is a paucity of data, however, on fission gas release from UN, with the available information restricted to pellet geometries with varying densities. Recoil ranges based on fission fragment energies were used to determine fission recoil release and higher temperature release data from irradiated high density UN fuel pellets were extrapolated to obtain diffusive release from UN kernels into the buffer region. The resulting computed particle pressures under operational temperature and elevated transient temperatures were used as input to thermomechanical models of particle behavior. The study assumed a full decoupling between the three outer layers (IPyC, SiC, and OPyC) and the kernel and buffer, therefore isolating the load bearing layers from any mechanical interaction with the kernel and buffer. At high fluence and burnup, the lack of knowledge for key material properties (especially kernel swelling rate and pyrocarbon strain rates) leaves room for such an assumption but it should also raise awareness that potential high swelling rates could affect the width of the buffer-IPyC gap, possibly leading to additional mechanical stress on the IPyC from the kernel and buffer.

The calculated particle internal pressures were used in conjunction with the COMSOL Multiphysics software to calculate the fluence dependent stress distributions generated within a TRISO particle. A measure of reliability of the TRISO particle was obtained by measuring the probability of survival of the SiC barrier layer and the maximum tensile stress generated in the pyrolytic carbon layers as a function of fluence. These reliability estimates were obtained as functions of the kernel diameter, buffer layer thickness, and pyrolytic carbon layer thicknesses. The SiC probability of survival increased with decreasing temperature, increasing buffer layer thickness, and increasing PyC thickness. The maximum tangential stress generated with the IPyC layer decreased significantly with increasing temperature but was relatively insensitive to changes in the buffer layer and PyC layer thicknesses. As a result of these competing effects, the best overall reliability based on internal gas pressure of the TRISO particle was achieved at lower temperatures and higher buffer layer thickness, with survival even at 1600 °C and 75 μm thickness buffer layer. In general, the conclusions are likely conservative given the high release fractions for the noble gases and the use of total vapor pressures over the condensed fission product phases.

Acknowledgements

This work was supported by the US Department of Energy, Office of Nuclear Energy, Fuel Cycle Research and Development Program. The authors wish to thank Stewart Voit, Kurt Terrani, Jeff Powers, David Petti and John Maki for valuable comments.

References

[1] K.A. Terrani, L.L. Snead, J.C. Gehin, J. Nucl. Mater. 427 (2012) 209.
[2] K.A. Terrani, J.O. Kiggans, Y. Katoh, K. Shimoda, F.C. Montgomery, B.L. Armstrong, C.M. Parish, T. Hinoki, J.D. Hunn, L.L. Snead, J. Nucl. Mater. 426 (2012) 268.
[3] S. Sunder, N.H. Miller, J. Alloys Compd. 271–273 (1998) 568.
[4] Y. Katoh, A. Kohyama, T. Nozawa, M. Sato, J. Nucl. Mater. 329 (2004) 587.
[5] S.M. Dong, Y. Katoh, A. Kohyama, J. Am. Ceram. Soc. 86 (1) (2003) 26.
[6] T. Koyanagi, S. Kondo, T. Hinoki, J. Nucl. Mater. 417 (2011) 435.
[7] H. Kishimoto, K. Ozawa, O. Hashitomi, A. Kohyama, J. Nucl. Mater. 367–370 (2007) 748.
[8] S.C. Weaver, R.L. Senn, J.L. Scott, B.H. Montgomery, Effects of Irradiation on Uranium Nitride Under Space-Reactor Conditions, ORNL-4461, 1973.
[9] M.A. DeCrescente, M.S. Freed, S.D. Caplow, Uranium Nitride Fuel, Development SNAP-50, PWAC-488, 1963, pp. 90–92.
[10] E.K. Storms, J. Nucl. Mater. 158 (1988) 119.
[11] A.A. Bauer, React. Technol. 15 (1972) 87.
[12] A.A. Bauer, J.B. Brown, E.O. Fromm, V.W. Storhok, Mixed-Nitride Fuel Irradiation Performance, in: Proc. ANS Conf, on Fast Reactor Fuel Element Technology, Materials Science and Technology Division, 1971, pp. 785–818.
[13] K. Tanaka, K. Maeda, K. Katsuyama, M. Inoue, T. Iwai, Y. Arai, J. Nucl. Mater. 327 (2004) 77.
[14] B. Feng, A. Karahan, S. Kazimi, J. Nucl. Mater. 427 (2012) 30.
[15] B.J. Lewis, J. Nucl. Mater. 148 (1987) 28.
[16] C. Wise, J. Nucl. Mater. 136 (1985) 30.
[17] L.C. Northcliffe, R.F. Schilling, Nuclear Data Tables, A7 Academic Press, New York, 1970, pp. 233–463.
[18] D.R. Olander, Fundamental Aspects of Nuclear Fuel Elements, Technical Information Center, Energy Research and Development Administration, 1976, pp. 293 and 301.
[19] G.K. Miller, D.A. Petti, J.T. Maki, D.L. Knudson, 2009, PARFUME Theory and Model Basis Report, INL/EXT-08-14497, Idaho National Laboratory, September 2009.
[20] A.H. Booth, "A Method of Calculating Fission Gas Diffusion from UO2 Fuel and Its Application to the X-2-f Loop Test", CRDC-721, Atomic Energy of Canada Limited, Report 496, September 1957.
[21] International Atomic Energy Agency, "High Temperature Gas Cooled Reactor Fuels and Materials", TECDOC-1645, March 2010.
[22] N.M. George, I. Maldonado, K.A. Terrani, A. Godfrey, J. Gehin, Neutronics Studies of Uranium-based Fully Ceramic Micro-encapsulated Fuel for PWRs, PHYSOR 2012, Knoxville, Tennessee, USA, April 15–20, 2012.
[23] C.W. Bale, P. Chartrand, S.A. Degterov, K. Eriksson, K. Hack, R.B. Mahfoud, J. Melancon, A.D. Pelton, S. Petersen, Calphad 26 (2002) 89–228.
[24] T.M. Besmann, D. Shin, T.B. Lindemer, J. Nucl. Mater. 427 (2012) 162.
[25] G.K. Miller, Ralph G. Bennett, J. Nucl. Mater. 206 (1993) 35.
[26] G.K. Miller, J. Nucl. Sci. Technol. 32 (1995) 989.
[27] G.K. Miller, J.T. Maki, D.L. Knudson, D.A. Petti, Current Capabilities of the Fuel Performance Modeling Code PARFUME, INEEL/CON-04-02240 September 22, 2004.
[28] G.K. Miller, D.A. Petti, John T. Maki, Darrell L. Knudson, J. Nucl. Mater. 374 (2008) 129.
[29] G.K. Miller, D.A. Petti, J.T. Maki, Development of an Integrated Performance Model for Triso-Coated Gas Reactor Particle Fuel, INEEL/CON-01-01553, HTR 2002 Conference, April 22–24, 2002.
[30] B. Boer, R. Sonat, Sen, M.A. Pope, A.M. Ougouag, Material Performance of Fully-Ceramic Micro- Encapsulated Fuel Under Selected LWR Design Basis Scenarios: Final, Report September 2011, INL/EXT-11-23313.
[31] International Atomic Energy Agency Report entitled, "Advances in High Temperature Gas Cooled Reactor Fuel Technology", Chapter 9. Benchmarking of Fuel Performance Models During Normal Operation and Operational Transients", IEAE-TECDOC-1674, Vienna: International Atomic Energy Agency, 2012.